Electronic Supplementary Material (ESI) for Journal of Materials Chemistry C.

Supporting Information for "Designing hierarchical structures of complex electronically conducting organic polymers via one-step electro-polymerization"

Tharindu A. Ranathunge, † Duong Ngo,† Dilan Karunarathilaka,† Nuwan H. Attanayake,‡ Indika Chandrasiri,† Phillip Brodgon,† Jared H. Delcamp,† R. M. Gamini Rajapakse,† and Davita L. Watkins†

†Department of Chemistry and Biochemistry, University of Mississippi, University, MS 38677-1848, USA

‡Department of Chemistry, Temple University, 1901 North 13th Street, Philadelphia, Pennsylvania 19122, USA.

*To whom correspondence should be addressed: dwatkins@olemiss.edu; rmgr@pdn.ac.lk

Table of Contents Pages

General Summary: Reagents and solvents were purchased from commercial sources and used without further purification unless otherwise specified. Thin layer chromatography (TLC) was performed on SiO2-60 F254 aluminum plates with visualization by UV light or staining. Flash column chromatography was performed using Purasil SiO2-60, 230–400 mesh from Fisher. Fluorine doped tin oxide (FTO) glass plates (surface resistance 7Ω/sq) were purchased from Sigma Aldrich. ^{1}H NMR spectra were recorded on a Bruker Avance DRX-500 (500 MHz spectrometer) and a Bruker Avance-300 (300 MHz) spectrometer and were reported in ppm using solvent as an internal standard (TMS). Chemical shifts (δ) are given in parts per million (ppm) relative to TMS and referenced to residual protonated solvent purchased from Cambridge Isotope Laboratories, Inc. ($CDCl_3$: δH 7.26 ppm; DMSO-d$_6$: δH 2.50 ppm). Data reported as: s = singlet, d = doublet, t = triplet, q = quartet, p = pentet, m = multiplet, b = broad, ap = apparent; coupling constant(s) in Hz; integration.

Synthesis of monomers

Synthesis of TTDT$_2$ has been reported in our previous study.[1] T$_3$ and DPPT$_2$ were synthesized based on reported work.[2-5] All NMR correlated to those reported studies.

Synthesis of DPPF$_2$

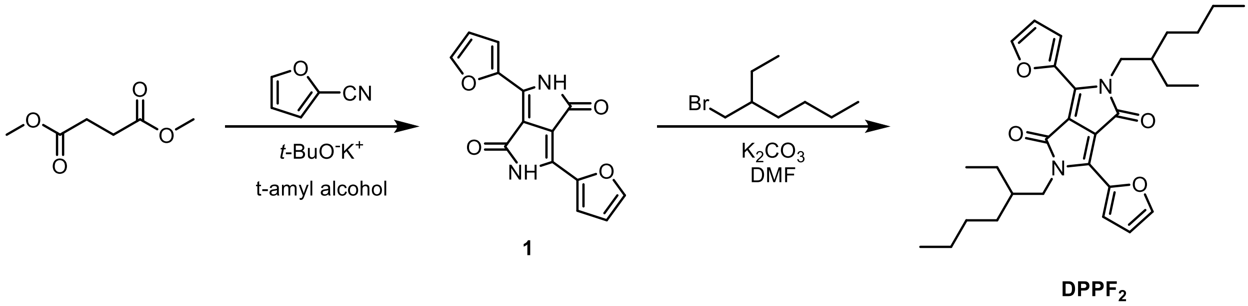

3,6-di(furan-2-yl)-2,5-dihydropyrrolo[3,4-*c*]pyrrole-1,4-dione (1).

Under nitrogen, Potassium *tert*-butylate (2.98 g, 26.6 mmol) was added to *t*-amyl alcohol (25 mL) in a 3 neck round bottom flask. 2-furancarbonitrile (2 g, 21.5 mmol) was added. The reaction was protected from light and heated until reflux. A solution of dimethyl succinate (1.74 g, 0.01 mol) in *t*-amyl alcohol (5.5 mL) wad added dropwise over 1 hour and the mixture was allowed to stir overnight. Then, the mixture was cooled to 50˚C and added with methanol (60 mL) and acetic acid (8 mL). The mixture was heated to 130˚C for 30 minutes then cooled to room temperature and vacuum filtered. The solid was collected washed with methanol and water to obtain the pure product as a dark purple powder (1.5 g, 56%): ^{1}H NMR (300 MHz, DMSO-*d*$_6$) δ 11.19 (d, *J* = 4.2 Hz, 2H), 8.05 (d, *J* = 3.7 Hz, 2H), 7.66 (d, *J* = 3.7 Hz, 2H), 6.84 (dd, *J* = 4.9, 2.7 Hz, 2H).

2,5-bis(2-ethylhexyl)-3,6-di(furan-2-yl)-2,5-dihydropyrrolo[3,4-*c*]pyrrole-1,4-dione (DPPF$_2$).

Under nitrogen, 2-Ethylhexylbromide (0.48 mL, 2.9 mmol) was added to a mixture of compound **1** (0.3 g, 1.12 mmol), anhydrous potassium carbonate (0.464 g, 3.36 mmol), and DMF (10 mL) in a 2-neck round bottom flask. The mixture was stirred at 140˚C overnight. After cooling to room temperature, the solution was quenched with 0.1 M HCl and extracted with diethyl ether. The organic layer was dried over Na_2SO_4 and concentrated under reduced pressure. Pure produce was obtained as a red solid in 27% yield (153 mg): ^{1}H NMR (500 MHz, Chloroform-*d*) δ 7.98 (d, *J* = 3.6 Hz, 2H), 7.26 (d, *J* = 1.8 Hz, 2H), 6.34 (dd, *J* = 3.7, 1.8 Hz, 2H), 3.69 (dd, *J* = 7.5, 1.8 Hz, 4H), 1.10 – 0.37 (m, 30H).

NMR Analysis

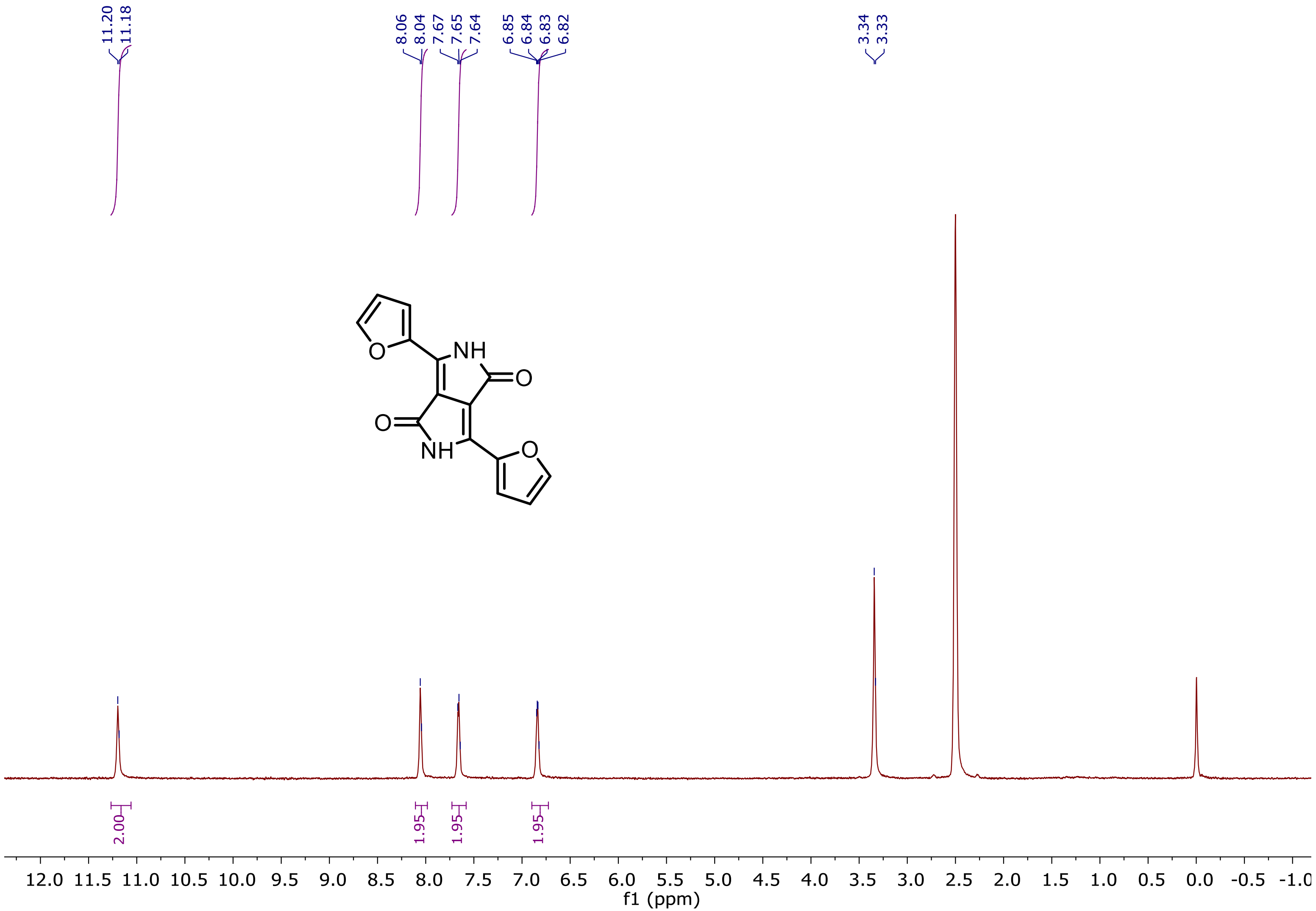

Figure S1. ^{1}H NMR spectrum of **1** (DMSO, 300 MHz).

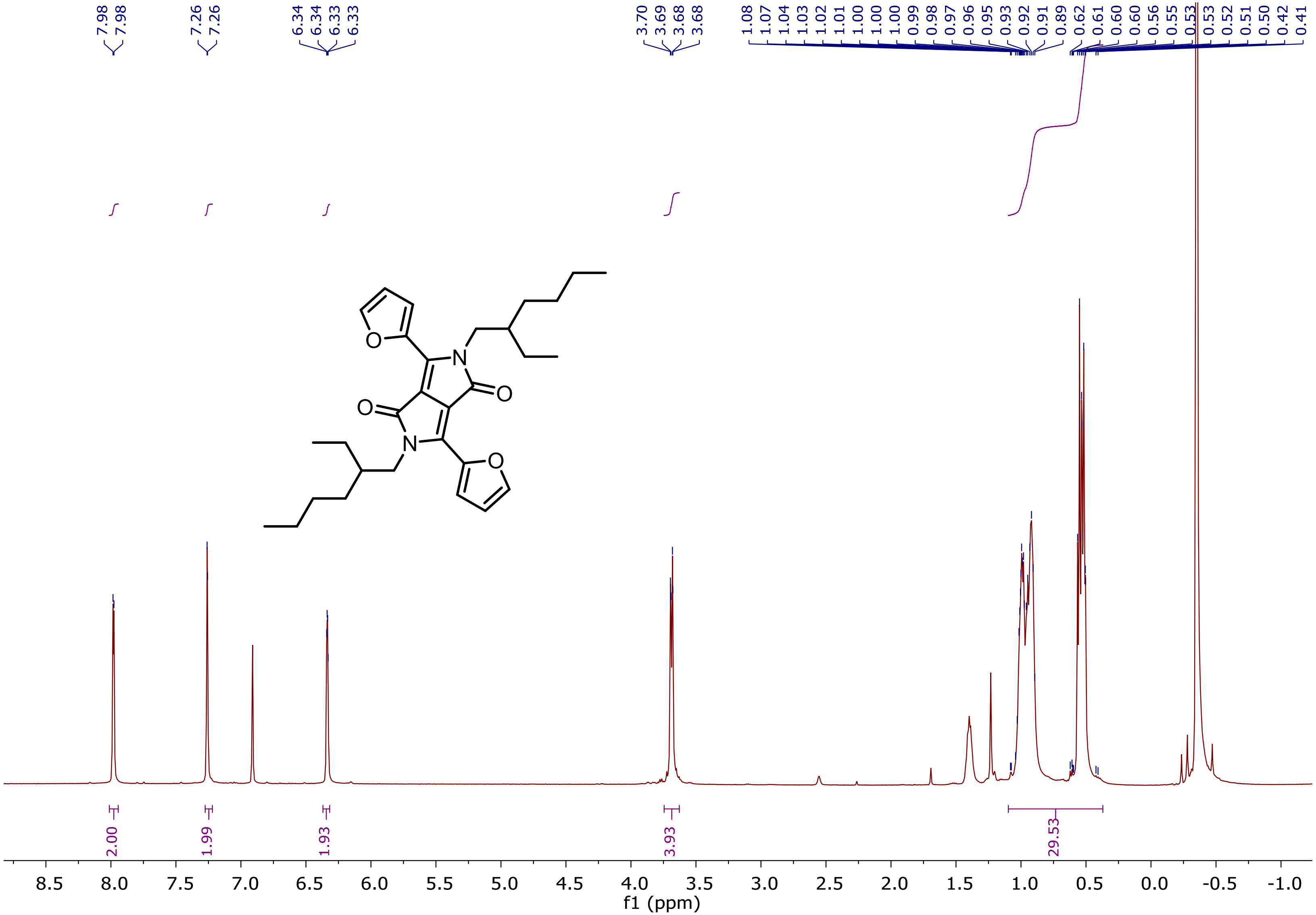

Figure S2. ^{1}H NMR spectrum of **DPPF**$_2$ (CDCl$_3$, 500 MHz).

Details of the Electropolymerization

Table S1. Preparation of **poly(T3-DPPT2-T3-TTDT2)**

Compound	Molar mass (g/mol)	Eq.	Mass	Amount	Volume
DPPT2	525	1	5.25 mg	1 mmol	-
T3	248	2	4.96 mg	2 mmol	-
TTDT2	475	1	4.75 mg	1 mmol	-
Tetrabutylammonium hexafluoro phosphate	387	100	387 mg	100 mmol	-
Acetonitrile anhydrous (98%)	41	-	-	-	10 ml

Table S2. Preparation of **poly(T3-DPPF2-T3-TTDT2)**

Compound	Molar mass (g/mol)	Eq.	Mass	Amount	Volume
DPPF2	498	1	4.92 mg	1 mmol	-
T3	248	2	4.96 mg	2 mmol	-
TTDT2	475	1	4.75 mg	1 mmol	-
Tetrabutylammonium hexafluoro phosphate	387	100	387 mg	100 mmol	-
Acetonitrile anhydrous (98%)	41	-	-	-	10 ml

Polymerisation and electrochemical characterisation of PolyT$_3$, Poly (T$_3$-TTDT$_2$), and Poly (T$_3$-TTDT$_2$) have been reported in our previous study.[6]

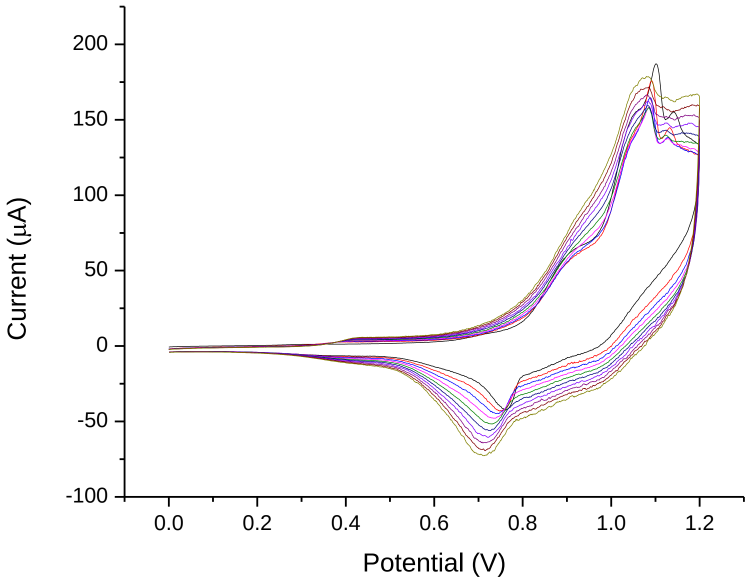

Figure S3. Successive CVs for the electro polymerisation of T$_3$-DPPF$_2$.

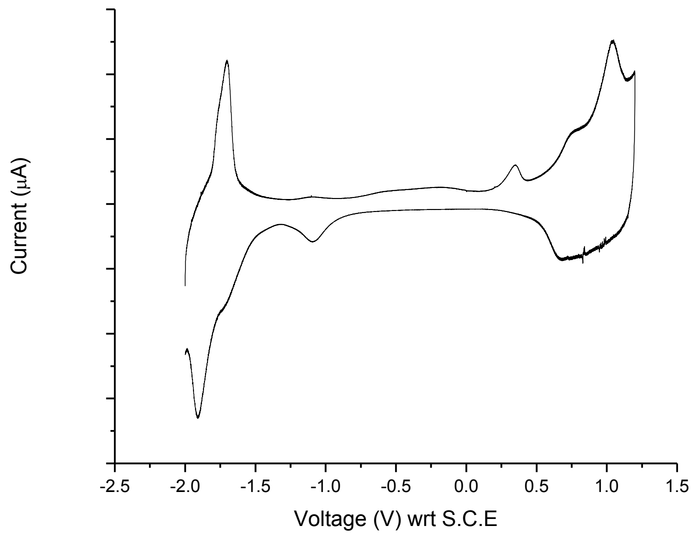

Figure S4. CV of poly**(**T_3-DPPF$_2$**)** in the BGE.

Segment 1:

peak potential (Ep), peak current (Ip), and electric charge (Ah)

Ep = -1.702 V ip = -2.604E-5 A Ah = -1.733E-5 C

Ep = -1.102 V ip = -1.201E-6 A Ah = -5.615E-7 C
Ep = 0.351 V ip = -7.786E-6 A Ah = -6.250E-6 C
Ep = 1.048 V ip = -2.342E-5 A Ah = -2.119E-5 C
Segment 2:
Ep = -1.094 V ip = 5.135E-6 A Ah = 5.019E-6 C
Ep = -1.911 V ip = 2.423E-5 A Ah = 1.624E-5 C

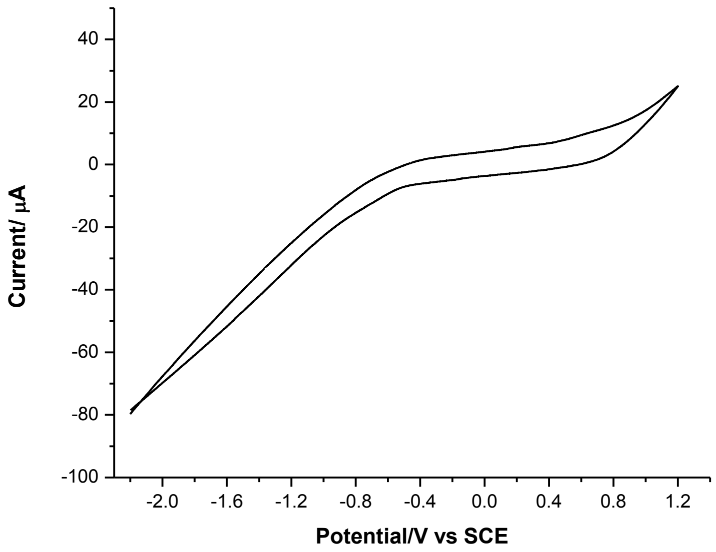

Figure S5. CV of $DPPF_2$ only in BGE; $DPPF_2$ was shown to be CV active but not capable of polymerization without T_3

peak potential (Ep) = 0.234 V   peak current (Ip) = 5.665E-8 A   electric charge (Ah) = 4.528E-8 C
Ep = 0.680 V   Ip = 4.973E-6 A   Ah = 5.311E-8 C

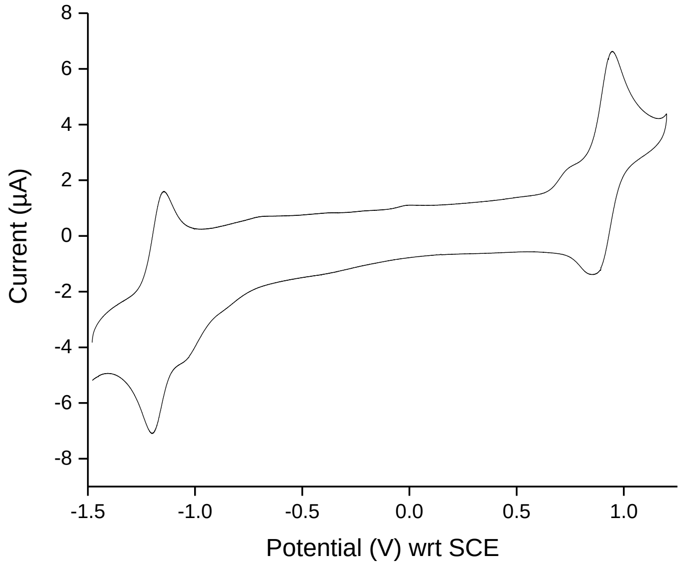

Figure S6. CV of $DPPT_2$ only in BGE;[6] $DPPT_2$ was shown to be CV active but not capable of polymerization without T_3

Segment 1:
Ep = -1.145 V   Ip = 3.058E-6 A   Ah = 1.886E-6 C
Ep = 0.000 V   Ip = 1.244E-7 A   Ah = 7.148E-8 C
Ep = 0.947 V   Ip = 3.360E-6 A   Ah = 2.069E-6 C
Segment 2:
Ep = 0.854 V   ip = -3.000E-6 A   Ah = -2.819E-6 C
Ep = -1.198 V   ip = -1.876E-6 A   Ah = -9.077E-7 C

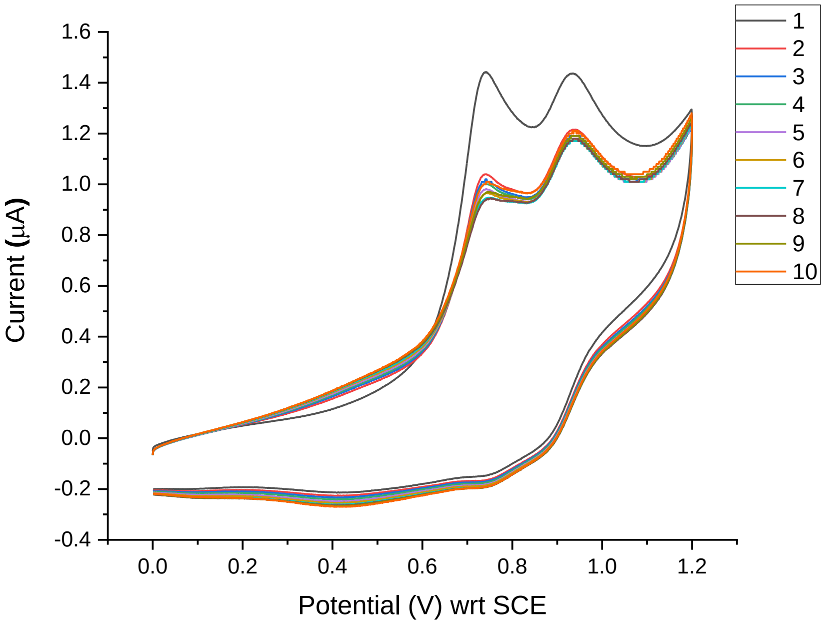

Figure S7. Successive CV's of $DPPT_2$ and $TTDT_2$ in a 1:1 mixture shows attempt of polymerization with decrease current respect to number of scans.

Table S3. Comparison of the significant onset peaks for polymers of interests

	Onset		Current		
	poly(T_3-$DPPT_2$-T_3-$TTDT_2$)	**poly(T_3-$DPPF_2$-T_3-$TTDT_2$)**	**poly(T_3-$DPPT_2$-T_3-$TTDT_2$)**	**poly(T_3-$DPPF_2$-T_3-$TTDT_2$)**	Current deviation
Positive regime onset 1	0.688 V	0.429 V	12.34 μA	51.06 μA	4.1377
Positive regime reverse onset 1	0.593 V	0.636 V	-5.39 μA	-39.55 μA	7.3376
Negative regime highest onset 1	-1.071 V	-1.708V	19.02 μA	111.3 μA	5.8517
Negative regime highest reversible onset 1	-1.141 V	-1.942 V	-21.35 μA	-122.6 μA	5.7423

	Onset		Current		
	poly(T_3-$DPPT_2$)	**poly(T_3-$DPPF_2$)**	**poly(T_3-$DPPT_2$)**	**poly(T_3-$DPPF_2$)**	Current deviation
Positive regime onset 1	0.644 V	0.347 V	11.24 μA	11.88 μA	1.05
Positive regime reverse onset 1	0.520 V	0.674 V	-6.43 μA	-16.96 μA	2.63
Negative regime highest onset 1	-1.080 V	-1.702V	25.07 μA	44.37 μA	1.84
Negative regime highest reversible onset 1	-1.17 V	-1.911 V	-30.94 μA	-66.14 μA	2.13

Nyquist plots

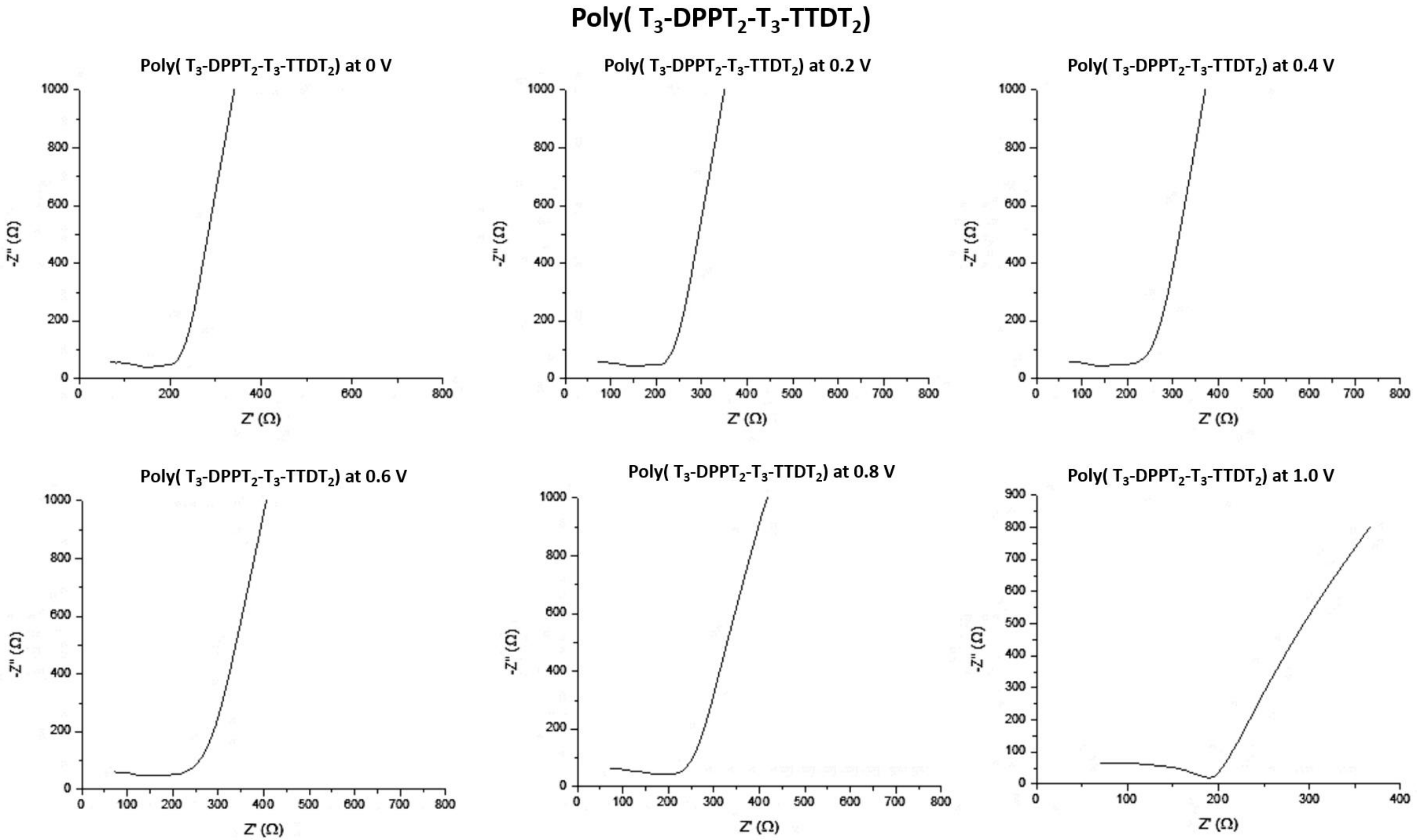

Figure S8. Nyquist plots for AC impedance analysis of poly(T_3-$DPPT_2$- T_3-$TTDT_2$) at varying frequencies (positive)

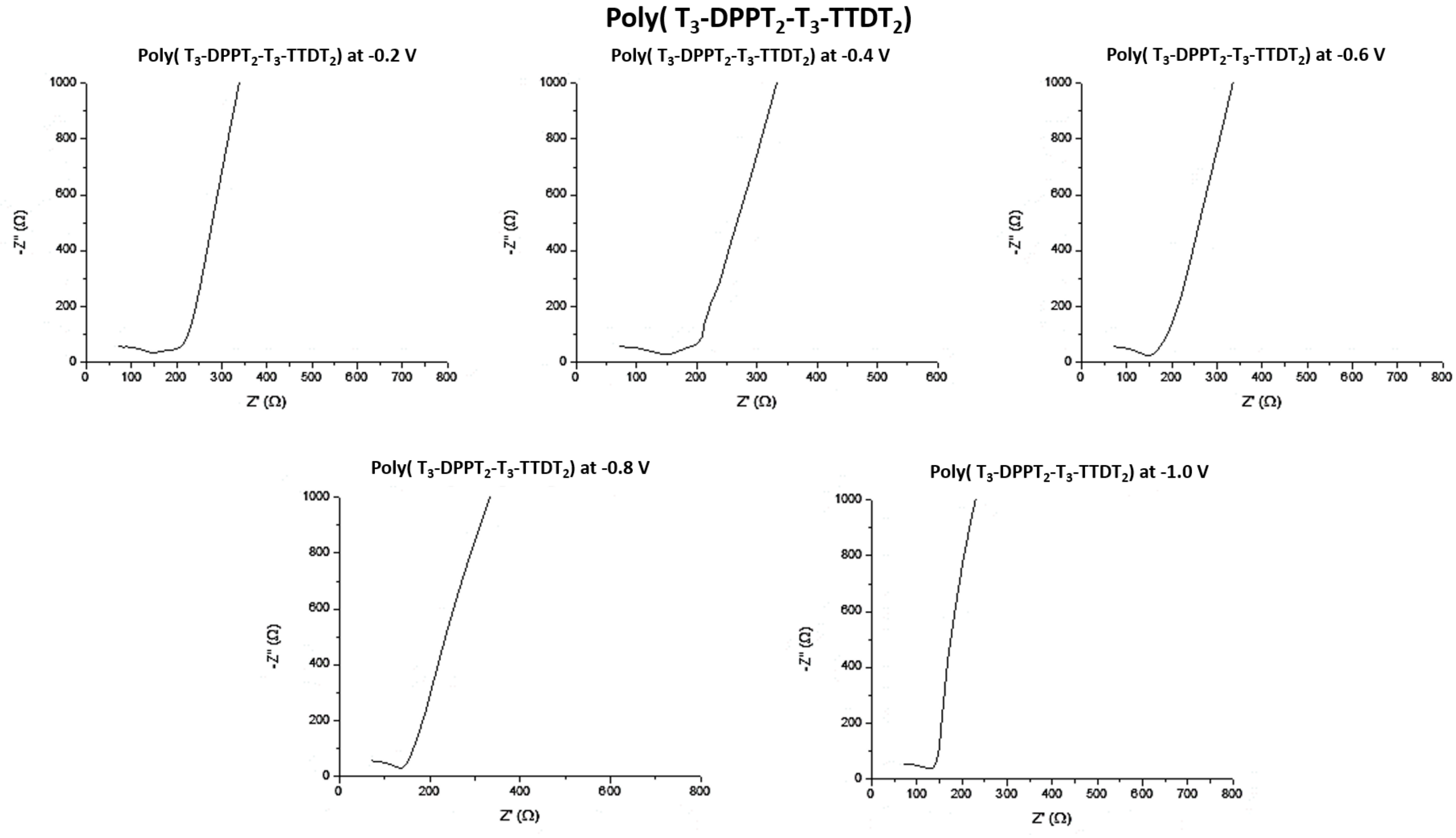

Figure S9. Nyquist plots for AC impedance analysis of poly(T$_3$-DPPT$_2$- T$_3$-TTDT$_2$) at varying frequencies (negative)

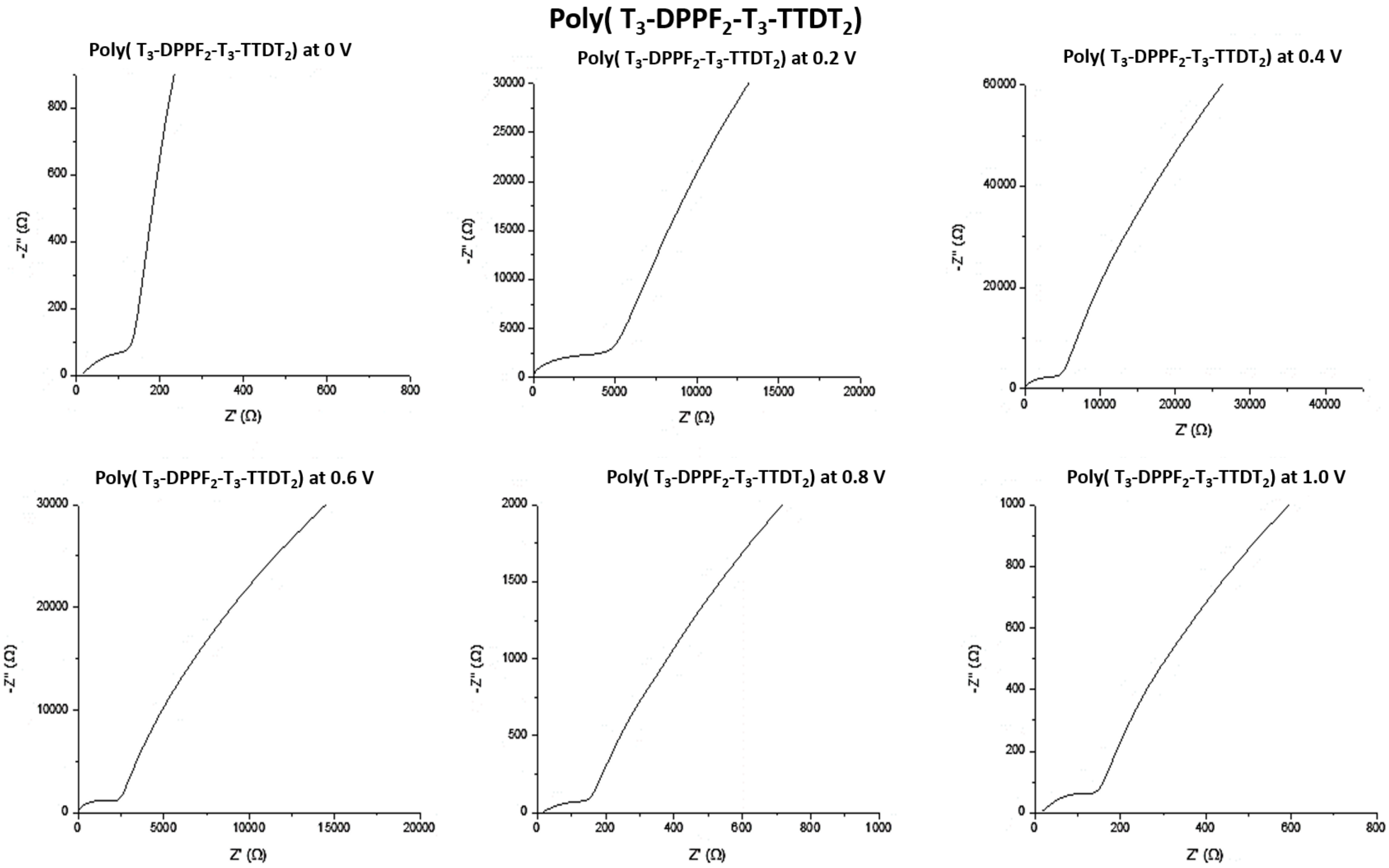

Figure S10. Nyquist plots for AC impedance analysis of poly(T$_3$-DPPF$_2$- T$_3$-TTDT$_2$) at varying frequencies (positive)

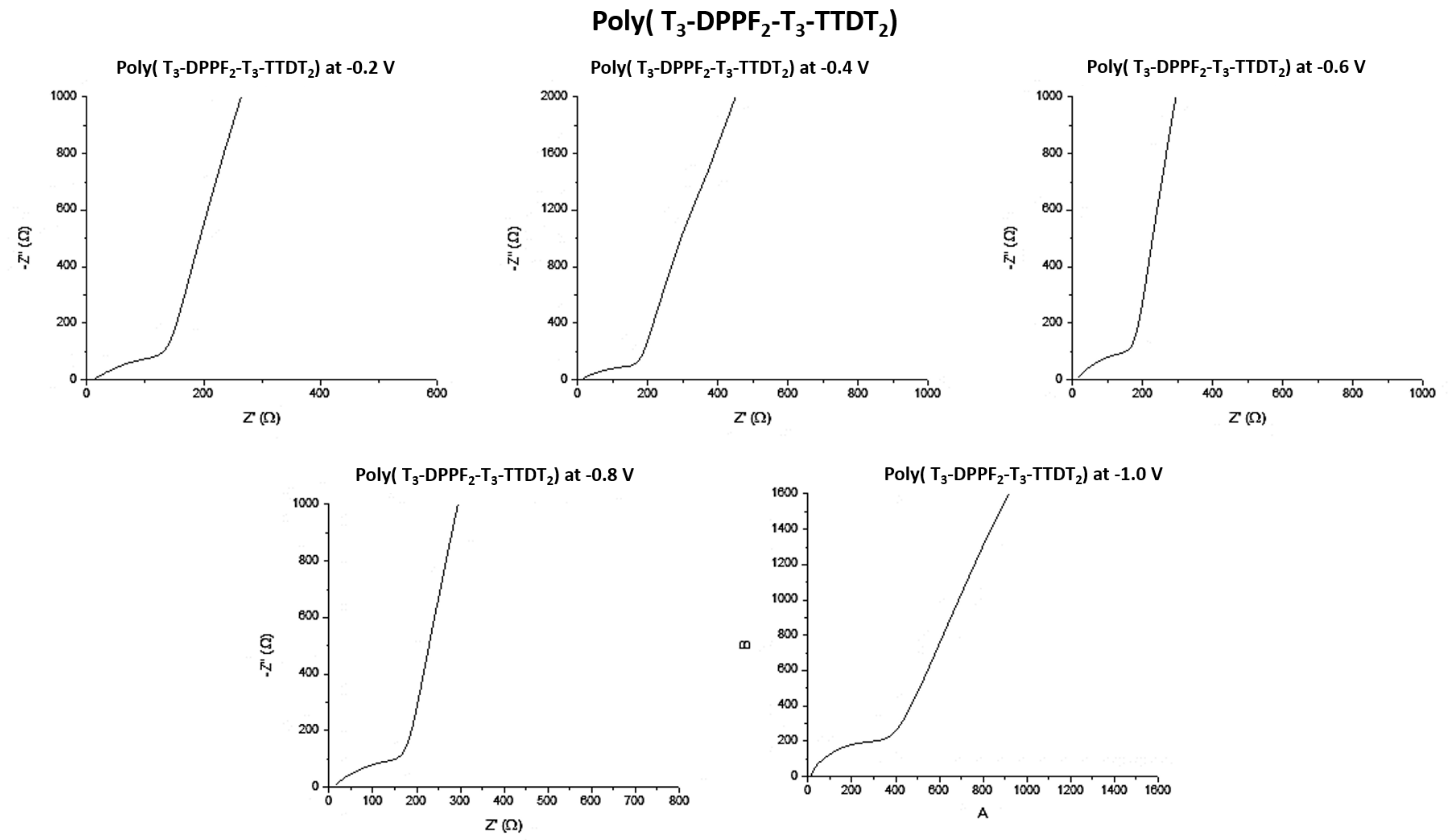

Figure S11. Nyquist plots for AC impedance analysis of poly(T_3-DPPF$_2$-TTDT$_2$) at varying frequencies (negative)

Poly(T_3-DPPF$_2$)

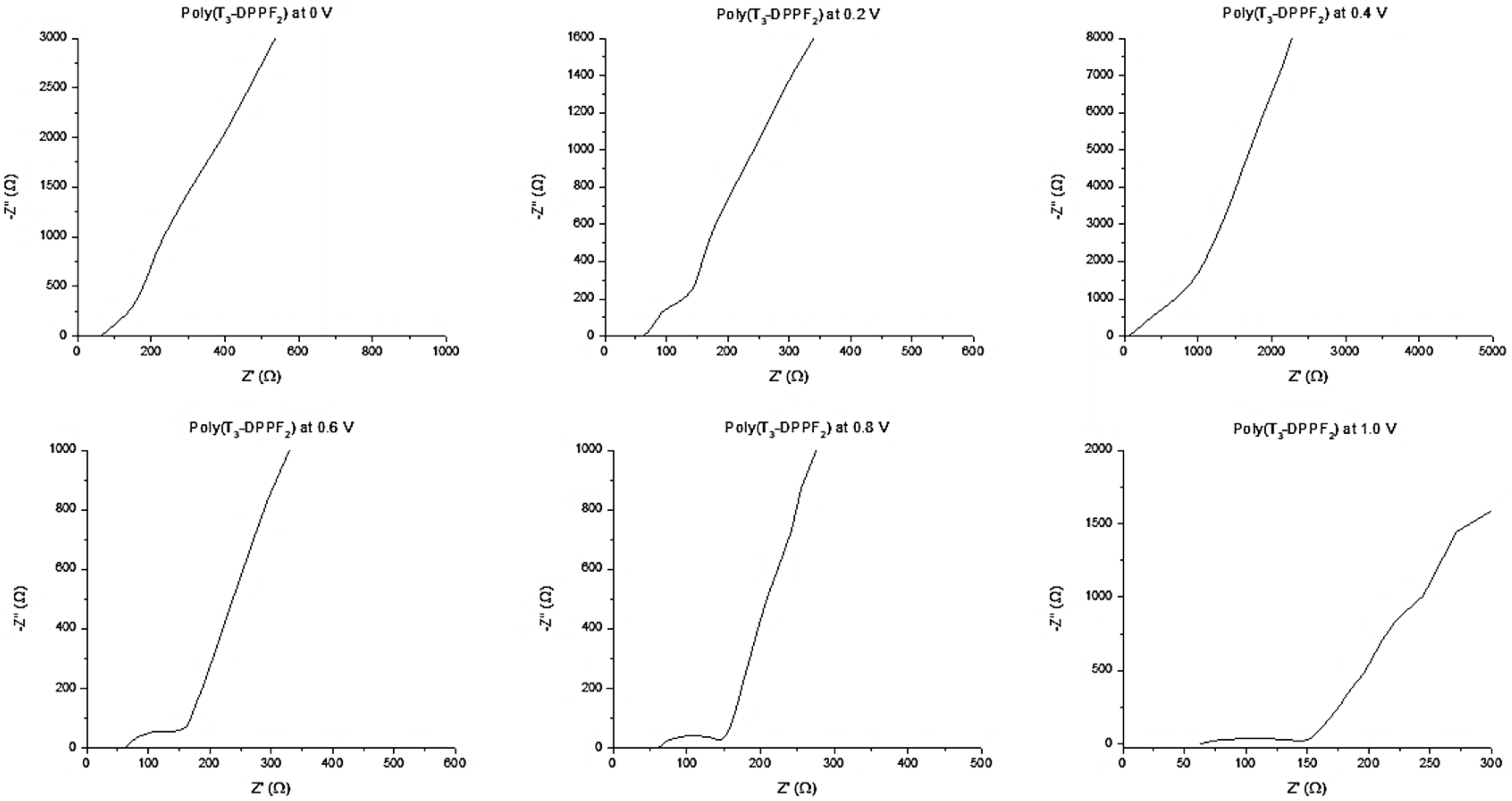

Figure S12. Nyquist plots for AC impedance analysis of poly(T_3-DPPF$_2$) at varying frequencies (positive)

Poly(T_3-$DPPF_2$)

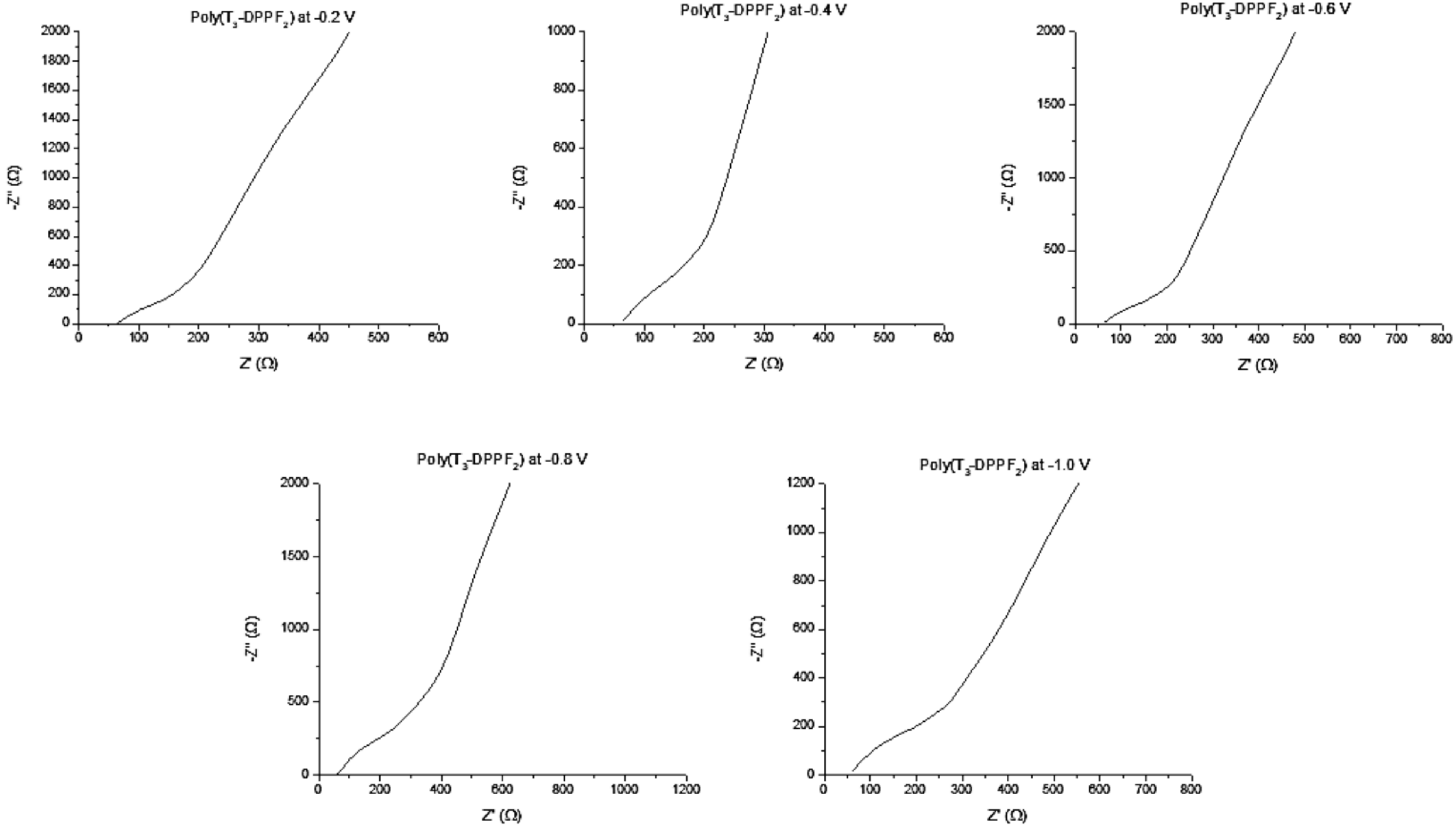

Figure S13. Nyquist plots for AC impedance analysis of poly(T_3-$DPPF_2$) at varying frequencies (negative)

Table S4. Electrical parameters extracted from Nyquist plots of AC impedance analyses of **poly(T_3-$DPPF_2$)** (top). Dual rail transmission line circuit (middle) and simplified equivalent circuit (bottom) used to extract data are also shown. [7-8]

DC Voltage (V)	R_s (Ω)	R_e (Ω)	C_d (μF)	W (μΩ)	C (μF)
-2	54.41	76.38	4.38E+00	14150	4.86E+02
-1.8	54.28	89.03	8.15E+00	17600	8.06E+02
-1.6	55.56	9.14E+01	5.39E+00	4411	2.10E+02
-1.4	48.97	1.00E+02	5.23E+00	785.2	7.31E+01
-1.2	39.69	1.53E+03	2.17E+02	494	1.12E+02
-1	38.29	1.68E+04	4.58E+01	530.6	5.64E+01
-0.8	40.84	3.79E+04	2.86E+01	615.7	2.56E+01
-0.6	48.17	3.17E+04	3.72E+01	707.9	2.14E+01
-0.4	49.34	2.64E+04	3.65E+01	783.8	2.03E+01
-0.2	51.13	2.20E+04	3.59E+01	921.1	2.06E+01
0	54.75	2.44E+04	2.86E+01	1300	1.81E+01
0.2	54.97	2.15E+04	2.28E+01	1492	2.19E+01
0.4	49.19	2.89E+02	7.94E+01	890.3	7.39E+01
0.6	60.97	5.86E+01	1.48E+01	4065	1.43E+02
0.8	63.41	7.20E+01	1.17E+01	15650	5.47E+02
1	64.21	7.41E+01	8.88E+00	25660	8.10E+02

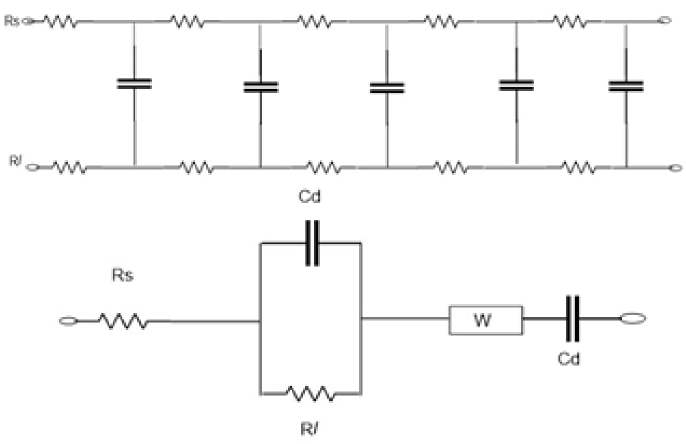

Figure S14. R_S-series resistance of the cell, R_e-resistance for electron transport along the polymer backbone, C_d-double layer capacitance between polymer-electrolyte interface, W-Warberg impedance for ingress and egress of counter ions by diffusion, C-capacitance of the high frequency pure capacitive regime.

SEM-EDX analysis

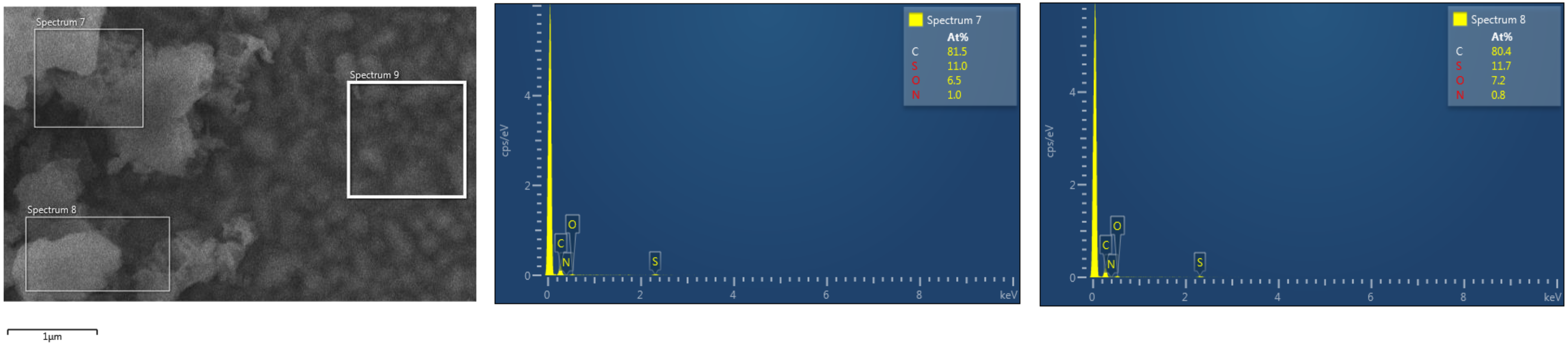

Figure S15. SEM image and SEM-EDX spot analysis of of T$_3$-DPPT$_2$- T$_3$-TTDT$_2$ n-type

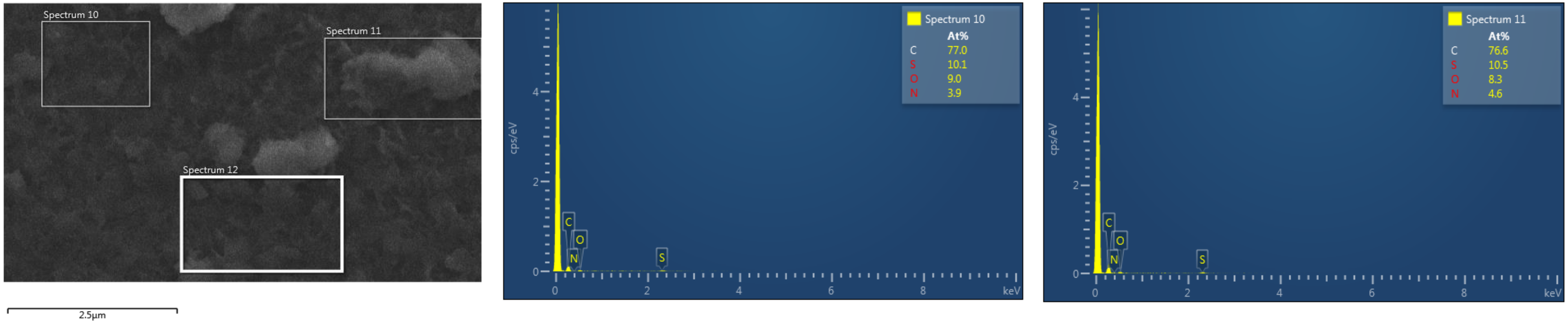

Figure S16. SEM image and SEM-EDX spot analysis of of T$_3$-DPPT$_2$- T$_3$-TTDT$_2$ p-type

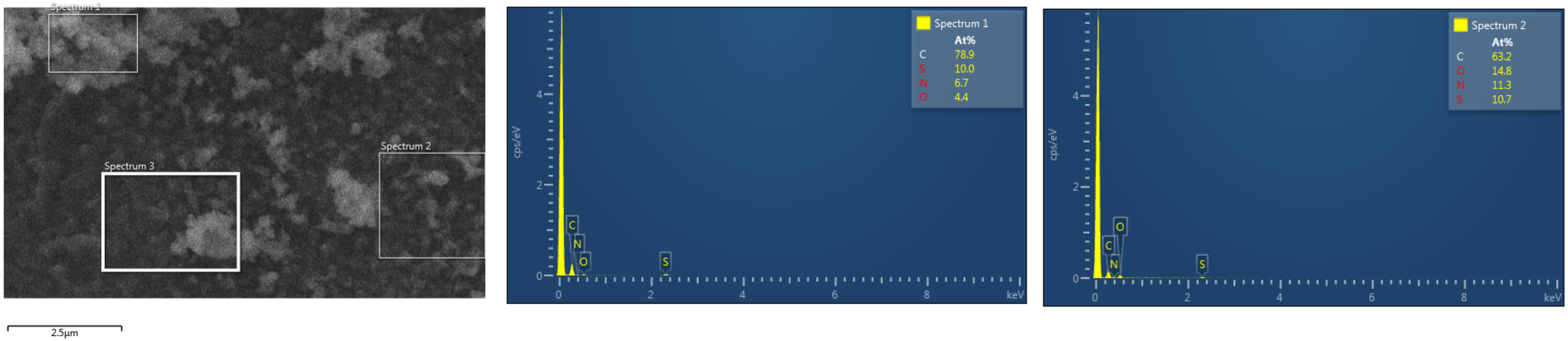

Figure S17. SEM image and SEM-EDX spot analysis of T_3-DPPF$_2$- T_3-TTDT$_2$ n-type

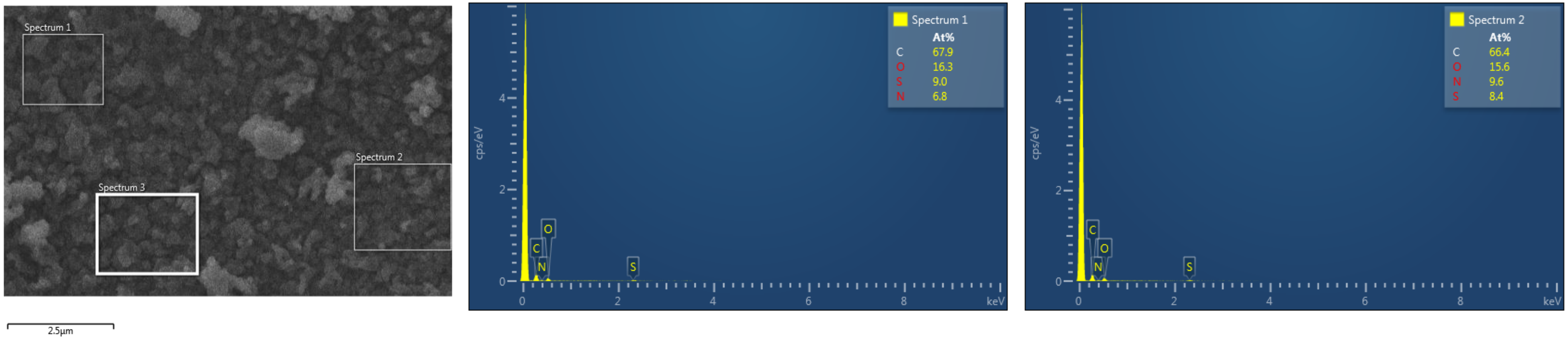

Figure S18. SEM image and SEM-EDX spot analysis of T_3-DPPF$_2$- T_3-TTDT$_2$ p-type

Table S5: Theoretical atomic ratios of diblock-copolymers

	Poly (TTDT$_2$-T$_3$)	Poly (DPPT$_2$-T$_3$)	Poly (DPPF$_2$-T$_3$)	TTDT$_2$	DPPT$_2$	DPPF$_2$
C	80.0%	82.3%	82.3%	80.0%	83.3%	83.3%
S	15.5%	9.80%	5.88%	13.3%	5.56%	0.00%
O	0.00%	3.92%	7.84%	0.00%	5.56%	11.1%
N	3.92%	3.92%	3.92%	6.67%	5.56%	5.56%

Optical data

UV−vis−NIR spectra were measured with a Cary 5000 instrument; energy level schematic derived from peak maximum and onset of peaks observed in the absorbance spectra. Second onset used unless otherwise noted. The onset was taken from the spectra and then the equation below was used to calculate the band gap. The data set or result was then extrapolated in graph form in which the y axis is E(eV).

Using the following equation,

Eg = 1240/ hv where Eg is energy gap and hv is wavelength.

Table S6. Absorbance λ_{max} for polymers made on FTO glass

Polymer	Positive Potential λ_{max} (nm) E_g (eV)	Onset (nm) E_g (eV)	Negative Potential λ_{max} (nm) E_g (eV)	Onset (nm) E_g (eV
poly(T$_3$-DPPT$_2$-T$_3$-TTDT$_2$)	390, 761, 1051$^{(S)}$, 1579 *3.18, 1.63, 1.18, 0.785*	581, 945, 1271, 1349(1st) *2.13, 1.31, 0.975, 0.919*	401, 769$^{(S)}$, 1058, 1564 *3.09, 1.61, 1.17, 0.793*	621, 861, 1252, 1331(1st) *1.99, 1.44, 0.99, 0.932*
poly(T$_3$-DPPF$_2$-T$_3$-TTDT$_2$)	361, 805, 1604 *3.43, 1.54, 0.773*	592, 1237, 1350 (1st) *2.09, 1.00, 0.918*	474, 879, 1552 *2.62, 1.41, 0.799*	586, 1285, 1354 (1st) *2.12, 0.965, 0.916*
poly(T$_3$-DPPF$_2$)	366, 689, 1116$^{(S)}$, 1538 *3.39, 1.79, 1.11, 0.806*	561, 905, 1305, 1401(1st) *2.21, 1.37, 0.950, 0.885*	404, 695$^{(S)}$, 1079$^{(S)}$, 1610, 1818$^{(S)}$ *3.07, 1.78, 1.15, 0.770, 0.682*	623, 850, 1310, 1399(1st), 1760, 1775(1st) *1.99, 1.46, 0.946, 0.886, 0.704, 0.698*

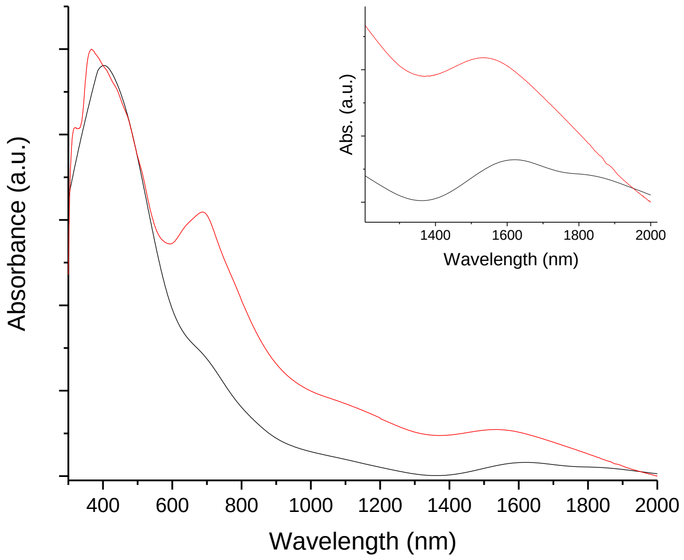

Figure S19. Absorbance spectra for Poly(T_3-DPPF$_2$); black line – n-type; red line – p-type

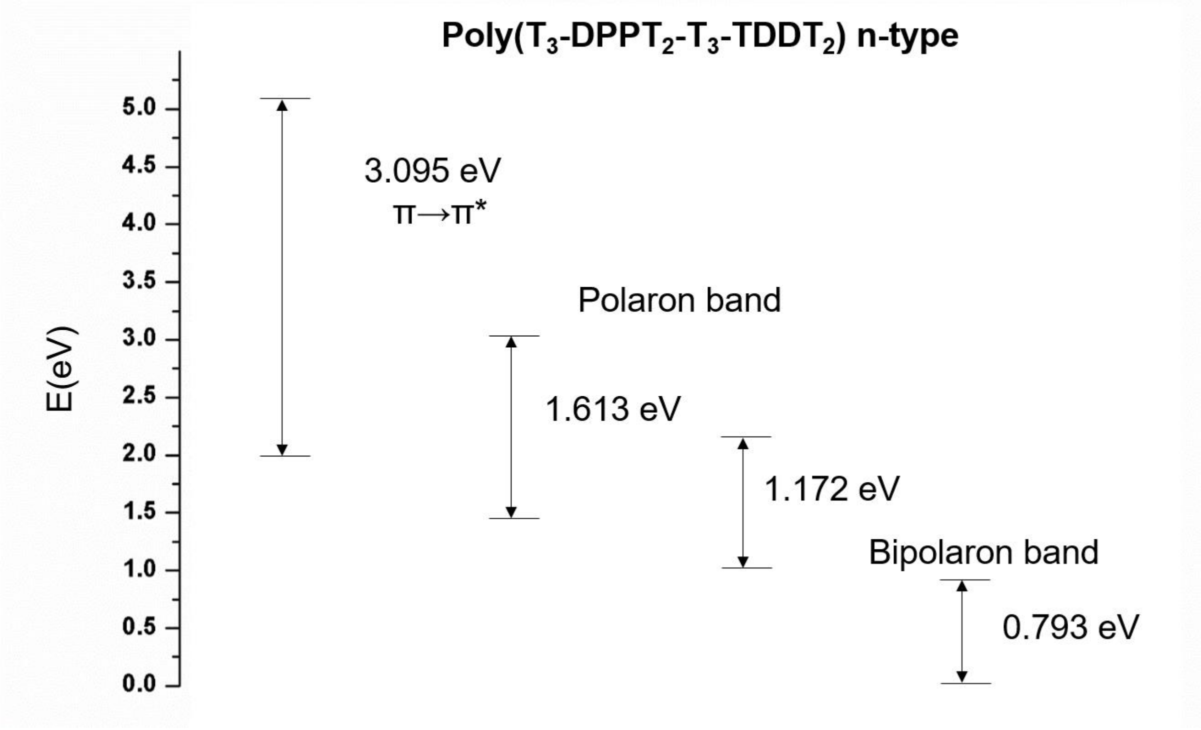

Figure S20. Schematic energy level diagrams for n-type poly(T_3-DPPT$_2$- T_3-TTDT$_2$)

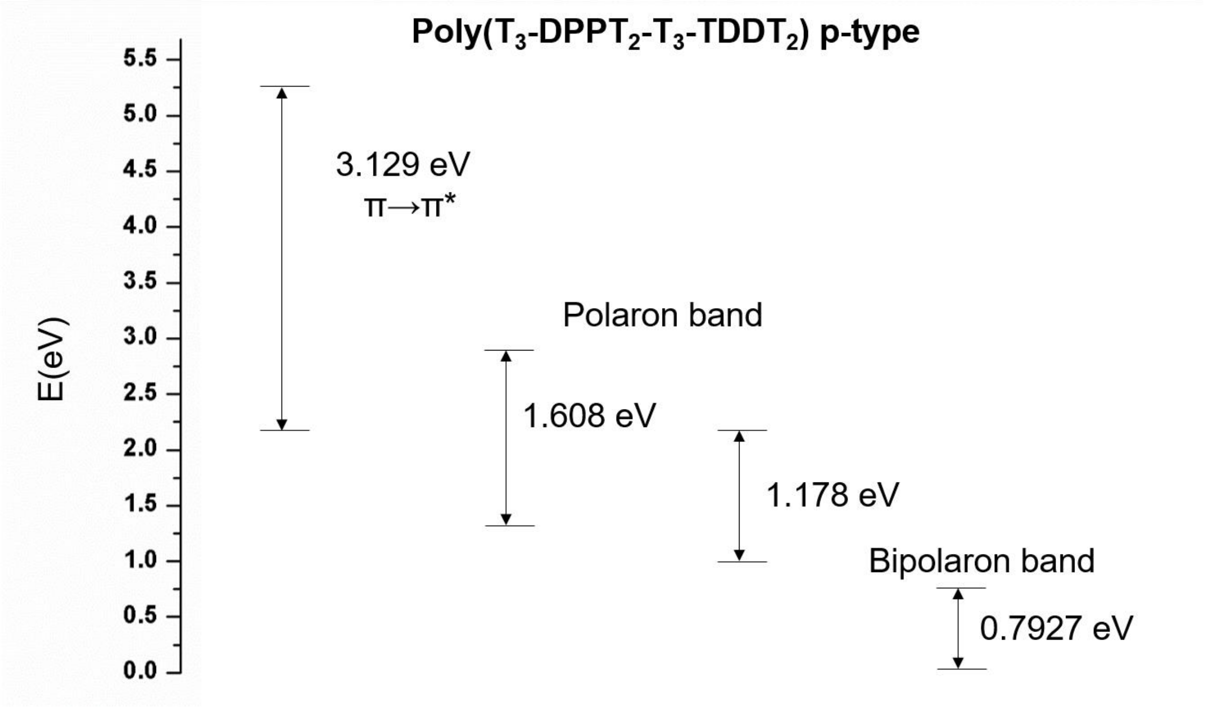

Figure S21. Schematic energy level diagrams for p-type poly(T_3-DPPT_2-T_3-TTDT_2)

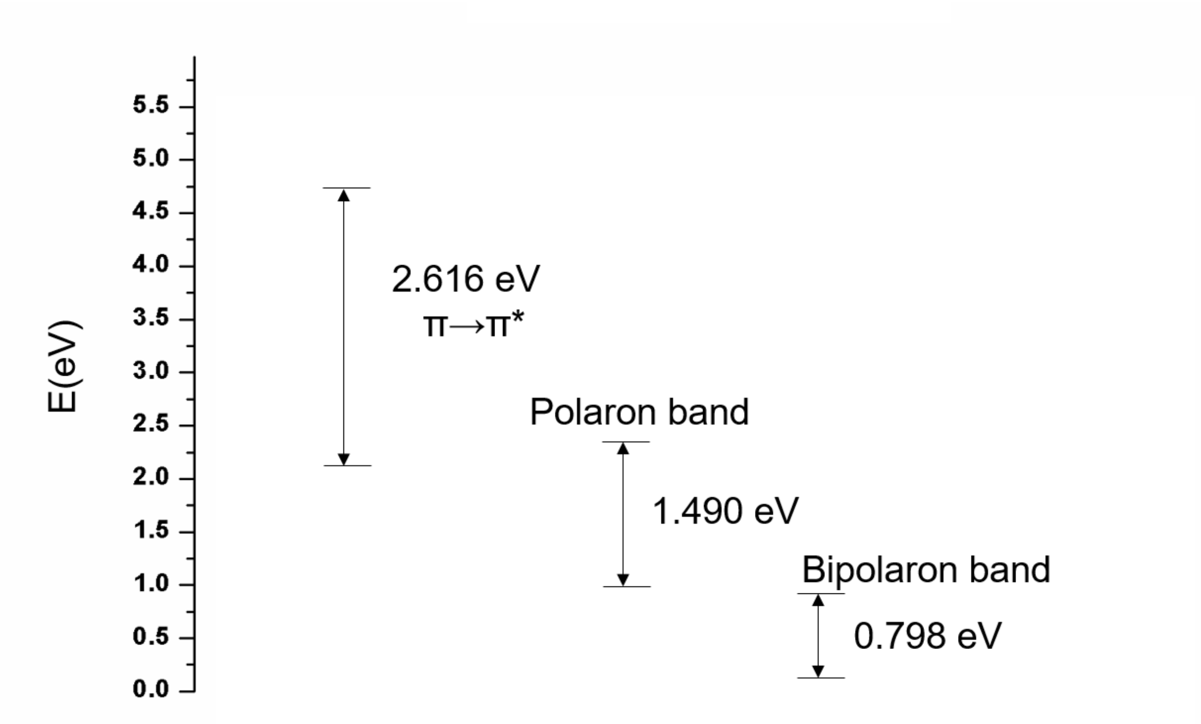

Figure S22. Schematic energy level diagrams for n-type poly(T_3-DPPF_2-T_3-TTDT_2)

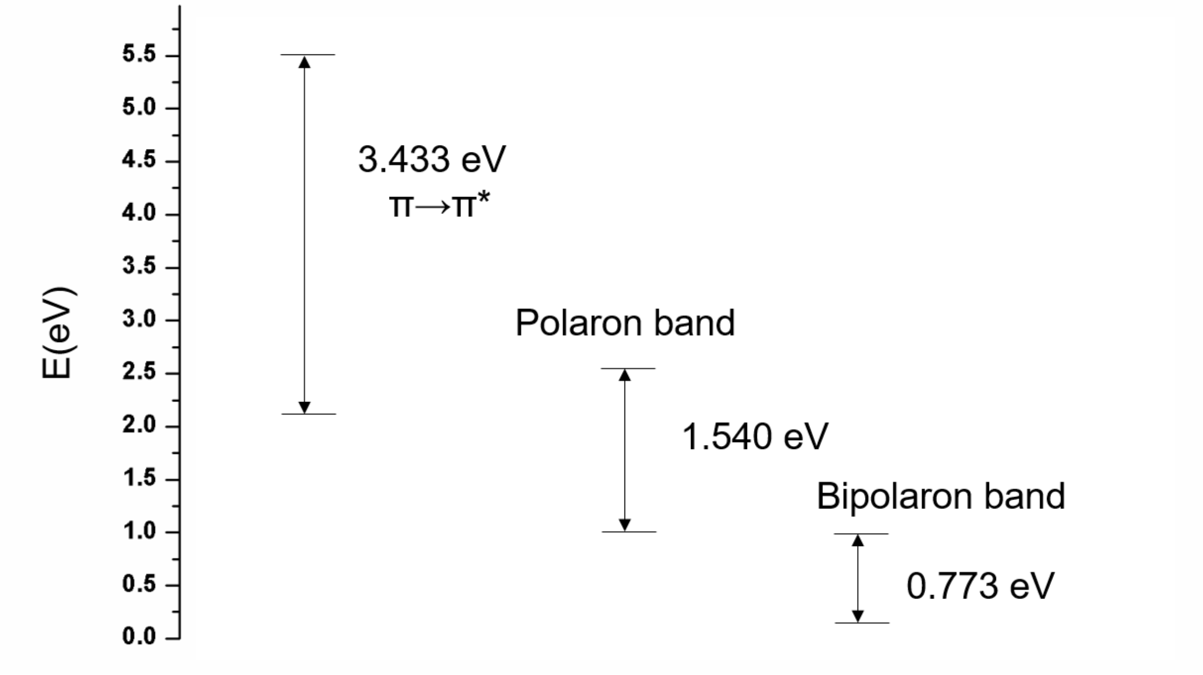

Figure S23. Schematic energy level diagrams for p-type poly(T_3-DPPF$_2$-T_3-TTDT$_2$)

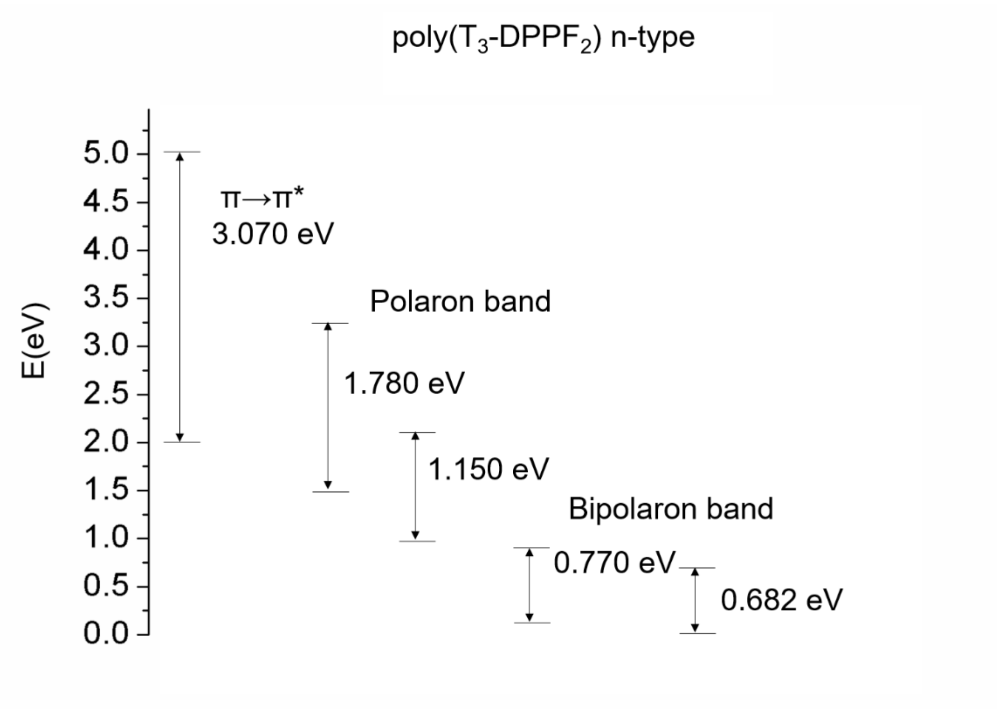

Figure S24. Schematic energy level diagrams for n-type poly(T_3-DPPF$_2$)

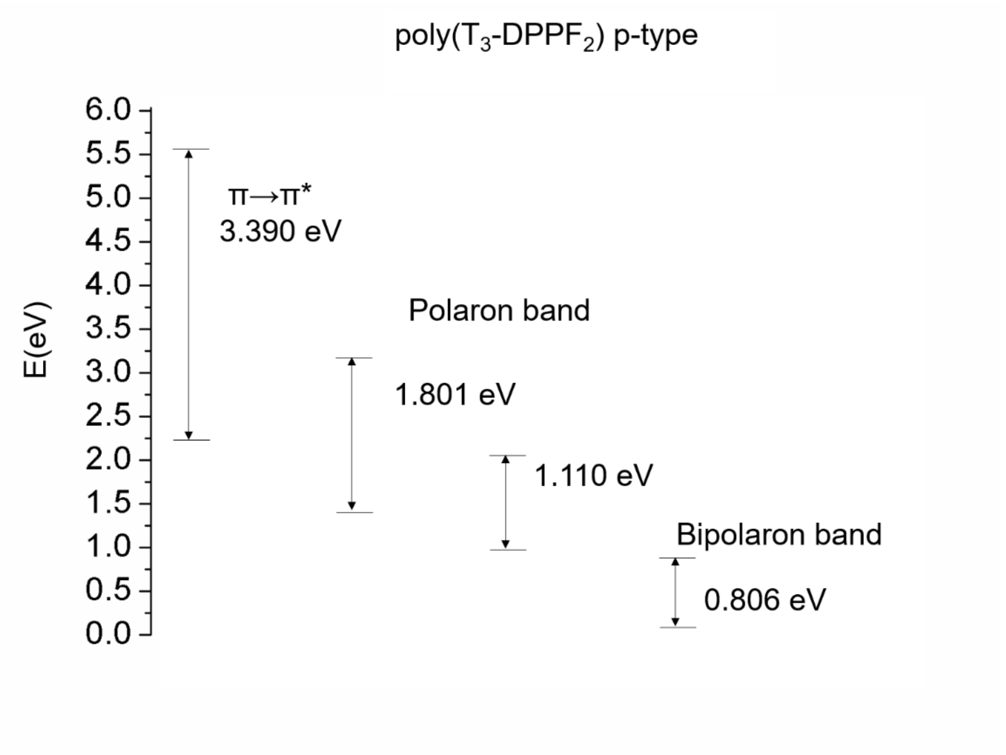

Figure S25. Schematic energy level diagrams for p-type poly(T_3-$DPPF_2$)

References

1. Zhang, Y.; Autry, S. A.; McNamara, L. E.; Nguyen, S. T.; Le, N.; Brogdon, P.; Watkins, D. L.; Hammer, N. I.; Delcamp, J. H., Near-Infrared Fluorescent Thienothiadiazole Dyes with Large Stokes Shifts and High Photostability. *The Journal of Organic Chemistry* **2017,** *82* (11), 5597-5606.
2. Kamal, M. R.; Al-taweel, S. A.; El-abadelah, M. M.; Abu Ajaj, K. M., SYNTHESIS OF α-THIOPHENE OLIGOMERS VIA ORGANOTIN COMPOUNDS. *Phosphorus, Sulfur, and Silicon and the Related Elements* **1997,** *126* (1), 65-74.
3. Fitzner, R.; Reinold, E.; Mishra, A.; Mena-Osteritz, E.; Ziehlke, H.; Körner, C.; Leo, K.; Riede, M.; Weil, M.; Tsaryova, O.; Weiß, A.; Uhrich, C.; Pfeiffer, M.; Bäuerle, P., Dicyanovinyl–Substituted Oligothiophenes: Structure-Property Relationships and Application in Vacuum-Processed Small Molecule Organic Solar Cells. *Advanced Functional Materials* **2011,** *21* (5), 897-910.
4. Podlesný, J.; Dokládalová, L.; Pytela, O.; Urbanec, A.; Klikar, M.; Almonasy, N.; Mikysek, T.; Jedryka, J.; Kityk, I. V.; Bureš, F., Structure–property relationships and third-order nonlinearities in diketopyrrolopyrrole based D–*π*–A–*π*–D molecules. *Beilstein Journal of Organic Chemistry* **2017,** *13*, 2374-2384.
5. Qian, G.; Qi, J.; Davey, J. A.; Wright, J. S.; Wang, Z. Y., Family of Diazapentalene Chromophores and Narrow-Band-Gap Polymers: Synthesis, Halochromism, Halofluorism, and Visible–Near Infrared Photodetectivity. *Chemistry of Materials* **2012,** *24* (12), 2364-2372.
6. Ranathunge, T. A.; Karunathilaka, D.; Ngo, D. T.; Attanayake, N. H.; Brodgon, P.; Delcamp, J. H.; Rajapakse, R. G.; Watkins, D. L., Radically Accessing D–A Type Ambipolar Copolymeric

Materials with Intrinsic Electrical Conductivity and Visible–Near Infrared Absorption Via Electro-Copolymerization. *Macromolecular Chemistry and Physics* **2019**, 1900289.

7. Lago, N.; Cester, A.; Wrachien, N.; Natali, M.; Quiroga, S. D.; Bonetti, S.; Barbato, M.; Rizzo, A.; Benvenuti, E.; Benfenati, V.; Muccini, M.; Toffanin, S.; Meneghesso, G., A physical-based equivalent circuit model for an organic/electrolyte interface. *Organic Electronics* **2016,** *35*, 176-185.

8. Guerrero, A.; Garcia-Belmonte, G.; Mora-Sero, I.; Bisquert, J.; Kang, Y. S.; Jacobsson, T. J.; Correa-Baena, J.-P.; Hagfeldt, A., Properties of Contact and Bulk Impedances in Hybrid Lead Halide Perovskite Solar Cells Including Inductive Loop Elements. *The Journal of Physical Chemistry C* **2016,** *120* (15), 8023-8032.